Oxid Met (2008) 69:1–12
DOI 10.1007/s11085-007-9080-z

ORIGINAL PAPER

Effect of Y Distribution on the Oxidation Kinetics of NiCoCrAlY Bond Coat Alloys

T. J. Nijdam · W. G. Sloof

Received: 16 April 2007 / Revised: 5 October 2007 / Published online: 22 December 2007

Abstract The relation between the Y distribution in the alloy and the growth kinetics of the developing oxide scale was studied for the thermal oxidation of two Ni–20Co–19Cr–24Al–0.2Y (at.%) alloys at 1,373 K: (i) a coarse-grain cast alloy with large Ni_5Y intermetallic precipitates, and (ii) a fine-grain freestanding coating with small Ni_5Y precipitates. Using a combination of experiments and model calculations, it is shown that the average growth kinetics of a NiCoCrAlY alloy are dependent on the size and distribution of Y-rich oxide inclusions (pegs) in the α-Al_2O_3 oxide layer. Alumina scales containing a high density of small Y-oxide inclusions grow faster than α-Al_2O_3 scales containing only a few, large Y-oxide inclusions. Upon oxidation of the freestanding coating, the Y-oxide inclusions in the scale attain their maximum size after the Y in the coating is completely consumed. After this point, a decrease in the average oxidation kinetics occurs.

Keywords Oxidation · Diffusion · Modeling · Alumina · MCrAlY bond coating

Introduction

High-temperature-coating systems, used in gas turbine engines, usually consist of a ceramic thermal barrier coating (TBC) on top, an intermediate metallic-bond coating (BC) and a superalloy substrate [1–5]. For the TBC usually yttria-stabilized zirconia (YSZ) is used. As bond coating either a Pt-modified Ni aluminide or a MCrAlY alloy (M = Ni and/or Co) is applied. During service, a thermally

T. J. Nijdam · W. G. Sloof
Netherlands Institute for Metals Research, Mekelweg 2, 2628 CD Delft, The Netherlands

T. J. Nijdam · W. G. Sloof (✉)
Department of Materials Science and Engineering, Delft University of Technology,
Mekelweg 2, 2628 CD Delft, The Netherlands
e-mail: w.g.sloof@tudelft.nl

grown oxide layer (TGO), develops between the TBC and the BC. The TGO is predominantly comprised of α-Al_2O_3 and provides protection of the underlying substrate against high-temperature corrosion. However, upon cooling of the component from high temperature, thermal-mismatch strains can develop within the TGO [5]. The elastic energy associated with these strains is the main driving force for failure of the coating system [5]. This strain energy increases with increasing TGO thickness. This explains that the failure of a high-temperature system can often be correlated with a critical TGO thickness at failure [6–8]. Thus, knowledge about the rate at which the TGO grows during service is necessary to predict the life span of the entire coating system.

The growth rate of a TGO scale is usually described with a simple parabolic rate law, since, the rate-limiting process in the growth of the oxide layer is generally the solid-state diffusion of anions and/or cations through the developing oxide layer [9, 10]. For the oxide scales developing on the Pt-modified Ni-aluminide bond coatings, parabolic growth kinetics usually apply [8, 11]. However, for the oxide scales developing on a MCrAlY bond coating, the growth kinetics cannot be described with a single parabolic rate constant, in particular when long oxidation periods are considered [12].

The fact that the oxide scales on MCrAlY alloys are not pure α-Al_2O_3, but also contain Y-rich oxide inclusions [13–18] may explain this deviation from parabolic growth kinetics. When the reactive element Y from the MCrAlY alloy becomes incorporated as Y-rich oxide inclusions in the α-Al_2O_3 scale, localized enhanced growth of the alumina around the Y inclusions occurs, resulting in the formation of protrusions (pegs) at the oxide/metal (O/M) interface. The size and density of these protrusions along the O/M interface depends on the distribution and the reservoir of the Y in the alloy [16, 17, 19]. This implies that when interpreting the oxidation kinetics of a MCrAlY alloy, the initial amount and distribution of the Y in the alloy have to be considered.

In this work, the relation between the Y distribution in the alloy and the growth kinetics of the developing oxide scale was investigated for the oxidation of a NiCoCrAlY alloy. To this end, the microstructures and growth kinetics of the oxide scales developing on two Ni–20Co–19Cr–24Al–0.2Y (at.%) alloys with different Y distribution were determined at 1,373 K. The experimental results are discussed with aid of a recently developed oxide-layer growth model that takes into account the effect of reactive-element-oxide inclusions on the growth rate of protective oxide scales [20].

Experimental Procedures

A cast Ni–20Co–19Cr–24Al–0.2Y (at.%) alloy and a free-standing Ni–20Co–19Cr–24Al–0.2Y coating, as deposited by electron-beam, physical-vapor deposition (EB-PVD), were prepared as described in Refs. [21, 18]. Disc-shaped specimens with a diameter of 15 mm and thicknesses of 2 mm for the cast alloy and 1 mm for the EB-PVD coating were cut using spark erosion. Next, both alloy surfaces were ground using a Buehler SiC paper with grit 1200 as the final step. Prior to oxidation,

all specimens were thoroughly cleaned with isopropanol and dried by blowing with compressed nitrogen.

Isothermal-oxidation experiments were preformed for 1, 25 and 100 h at a temperature of 1,373 K and a partial oxygen pressure of 10^5 Pa (1 atm.). The experiments were executed in a horizontal alumina tube furnace (Lenton PTF 16/75/610; inner diameter 75 mm) with pure oxygen passing through the furnace at a controlled flow rate of 1 l/min. Specimens were inserted into the furnace as rapidly as possible to minimize oxidation upon heating. After oxidation, specimens were transported quickly out of the furnace and allowed to cool in ambient air.

The cyclic-oxidation experiments were conducted in a furnace containing four ceramic tubes at the National Aerospace Laboratory (NLR, Marknesse, The Netherlands). For each alloy, three specimens were subjected to the following thermal cycles in laboratory air: 9 minutes heating, 45 min hot dwell at 1,373 K, and 10 min cooling (after 10 min the temperature was below 373 K). For each alloy, one of the three specimens was withdrawn from the test after 380 cycles. The other two specimens were tested up to 1,000 cycles, after which the test was stopped. Prior to cycling and after a certain number of cycles, the mass of each alloy (i.e. net mass change) was measured using a microbalance (accuracy $\sim$ 10 μg). The resulting mass-change data were averaged for each alloy and subsequently normalized with respect to specimen area.

After oxidation and examination of the oxide-surface morphology, oxide/alloy cross-sections were prepared using the procedure described in Ref. [22]. To reveal the oxide-layer microstructure in more detail, selected areas (with a size of about 0.5 $\times$ 0.5 mm) of the cross-sections were fine-polished by ion milling using a JEOL SM 09010 cross-section ion polisher [23]. To this end, a 5 kV Ar ion beam was employed.

Scanning-electron microscopy (SEM) was employed to determine the morphology and thickness of the oxide scales, the size of the Y-rich oxides in the scale, as well as the microstructure changes in the underlying alloys as a function of oxidation time (see section “Modeling and Data Analysis”). Energy-dispersive X-ray spectroscopy (EDXS) in combination with electron-backscatter-diffraction (EBSD) analysis was used to determine the phase constitution at selected points in the oxide scale. For this purpose, a JEOL JSM 6500F microscope was used, equipped with an Autrata [24] detector for observation of backscatter-electron (BSE) images, a Noran Pioneer 30 mm^2 Si(Li) detector for EDXS analysis, and a HKL Nordlys detector for the recording of electron-backscatter patterns (EBSP). The magnification of the microscope was calibrated such that the error in the length scale was less than 1%. The processing of the X-ray spectra and the EBSP was performed with a ThermoNoran Vantage system (version 2.3) and the HKL Technology Channel 5 (version 5.9) software, respectively.

Microstructural Observations

Prior to oxidation, both alloys have a multiphase microstructure, consisting of precipitates of the Al-rich β-NiAl phase in a matrix of the Al poor γ-Ni phase

(Fig. 1). The main difference between the microstructures of the two alloys is the size of the β precipitates (Fig. 1). The cast alloy contains much larger β precipitates than the EB-PVD coating. Besides a difference in β precipitate size, the alloys also exhibited a different distribution of Y. The reason for this is that the solubility of Y in NiCoCrAlY alloys is very low [15]. Electron-microprobe measurements indicate the solubility of Y in the two alloys was less than 0.02 at.% [21] (the detection limit of our electron-probe micro analyzer). Due to its low solubility, the Y was mostly confined within Ni_5Y precipitates along phase and/or grain boundaries in the alloy (as identified by X-ray diffraction [21]). The size of these Ni_5Y precipitates depends on the phase and/or grain-boundary density in the alloy. Thus, the Ni_5Y precipitates are much larger for the coarse-grain (low density of these boundaries) cast alloy than for the fine-grain (high density of these boundaries) EB-PVD coating.

Upon isothermal and cyclic oxidation, a double-layered oxide scale developed on both alloys, consisting of a thin, porous layer near the oxide surface and a thick, columnar-grain layer near the oxide/metal interface (Fig. 2). The thickness of the outer oxide layer was independent of the oxidation times studied, indicating that the oxide products in this layer were formed during initial oxidation (i.e. transient oxidation [25–27]). The transient oxide products were not identified, since this was not a focus of this study. The inner oxide layer in both cases consisted of α-Al_2O_3 (as identified by EBSD) and Y-rich oxide inclusions (Fig. 2). According to EDXS and EBSD analysis, two types of Y-rich oxides were formed (see inserts in Fig. 2): (i) a cubic oxide almost exclusively made up of Y and O, and (ii) a cubic oxide containing similar amounts of Y and Al next to O. Based on these results, it is concluded that the former is made up of Y_2O_3, while the latter is cubic $YAlO_3$ (i.e. with ideal perovskite structure). In some cases, a single oxide inclusion was composed of a core of Y_2O_3 surrounded by a sheath of $YAlO_3$ (see Fig. 2d). This result indicates that the $YAlO_3$ formed due to a solid-state reaction between Y_2O_3 and α-Al_2O_3.

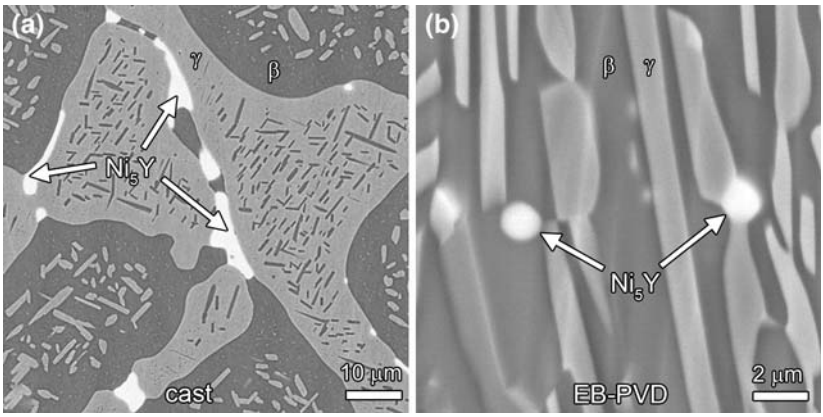

Fig. 1 Backscatter-electron images of the microstructures of the (**a**) cast and (**b**) EB-PVD Ni–20Co–19Cr–24Al–0.2Y alloy prior to oxidation. Notice the difference in magnification

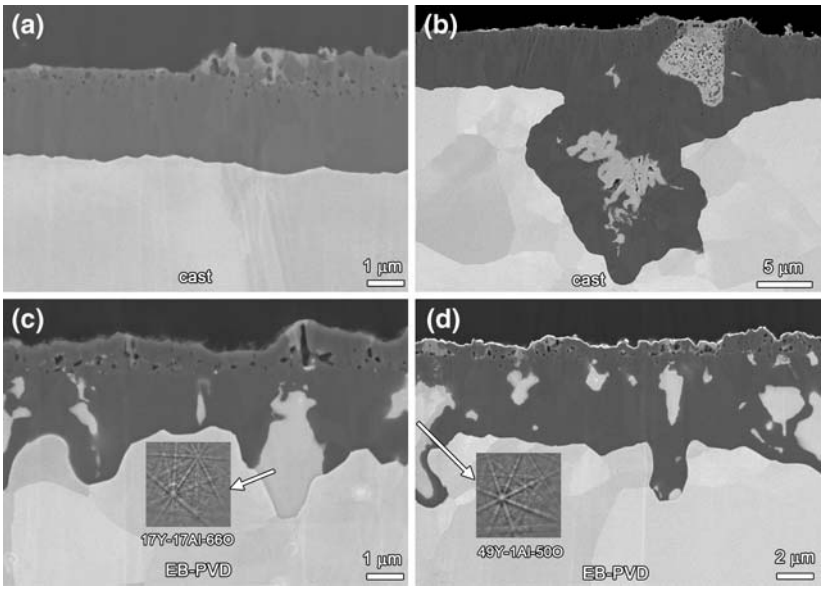

Fig. 2 Backscatter-electron images of the oxide/alloy cross-sections of the (**a**, **b**) cast, and (**c**, **d**) EB-PVD Ni–20Co–19Cr–24Al–0.2Y alloy after oxidation at 1,373 K. (**a**, **c**) 25 h isothermal oxidation, (**b**) 750 h cyclic oxidation, and (**d**) 285 h cyclic oxidation. The inserts show the compositions and electron backscatter patterns of the two indicated Y-rich oxide inclusions

The incorporation of the Y-rich oxide inclusions in the scale leads locally to enhanced growth of the oxide scale and consequently to a roughening of the oxide/metal interface. Clearly, the O/M interface is relatively smooth at those locations where Y-rich oxides are absent in the scale (Fig. 2a), and relatively rough at those positions where Y-rich oxide inclusions are present in the scale (Fig. 2b–d). The formation of these so-called protrusions (or pegs) at the O/M interface is a commonly observed phenomenon for the oxidation of MCrAlY alloys [17, 28] and coatings [13–16]. Close inspection of the location of the Y-rich oxide inclusions revealed that for both alloys almost all inclusions were formed above alloy grain or phase boundaries (Fig. 2), in agreement with previous reports [13, 17, 28, 29]. In some samples, internal oxidation of Y in advance of the O/M interface was observed, but the total amount of internally oxidized Y was very small compared with the amount of Y oxides within the scale.

Finally, the incorporation of Y as oxide inclusions in the scale leads to a depletion of the Y from the coating. As is clearly shown in Fig. 3, oxidation leads to a formation of an almost uniform zone free of Ni_5Y precipitates in the alloy region adjacent to the O/M interface.

Modeling and Data Analysis

A model was developed for describing the effect of Y-rich oxide inclusions on the oxidation kinetics of MCrAlY coating alloys. A schematic illustration of this model,

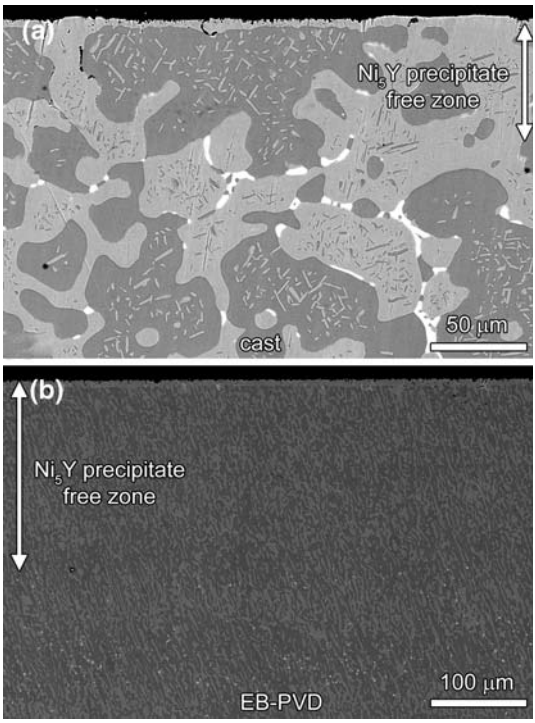

Fig. 3 Backscatter-electron images of the microstructure of the (**a**) cast and (**b**) EB-PVD Ni–20Co–19Cr–24Al–0.2Y alloy after 25 h of isothermal oxidation at 1,373 K. The bright spots correspond to the Ni_5Y precipitates

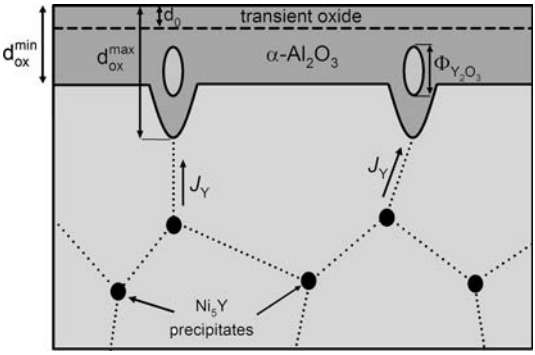

Fig. 4 Schematic illustration of the model used to determine the effect of the Y oxide inclusions on the growth kinetics of the NiCoCrAlY alloys

for which the details are provided in Ref. [20], is given in Fig. 4. The model was based on the following considerations:

(i) Following a short transient oxidation stage, the oxide scale forming between the protrusions consists solely of α-Al_2O_3. This alumina scale grows according to parabolic oxidation kinetics and is further referred to as the minimum oxide-scale thickness d_{ox}^{min}.

(ii) Above each alloy phase or grain boundary one protrusion (or peg) is formed. The thickness of the scale above the alloy grain boundaries is denoted as the

maximum oxide-scale thickness d_{ox}^{max}. The value of d_{ox}^{max} is taken equal to the value of d_{ox}^{min} plus the amount of Y_2O_3 ($\Phi_{Y_2O_3}$) within a single protrusion. Thus, the Y_2O_3 inclusions do not affect the growth rate of the alumina scale.

(iii) The amount of Y_2O_3 within a protrusion is taken equal to the maximum amount of Y that can be supplied by dissolution and diffusion of Y from Ni_5Y precipitates along alloy grain or phase boundaries to the oxide/metal interface during a given oxidation period.

(iv) The average oxide-scale thickness $\langle d_{ox} \rangle$ is considered to be a linear combination of scale thicknesses in between and on top of the alloy grain or phase boundaries (i.e. the values of d_{ox}^{min} and d_{ox}^{max}).

The model was applied to the oxidation of the cast and the EB-PVD Ni–20Co–19Cr–24Al–0.2Y alloys at 1,373 K. To calculate the oxidation kinetics of the two alloys, the following data are required: the molar volume of the alloy, the molar volume of Y_2O_3, the parabolic rate constant of α-Al_2O_3, the boundary diffusion coefficient of Y in the alloy, the Y content in the alloy, the solubility of Y in the alloy, the size of the β precipitates and the size of the Ni_5Y precipitates in the alloy. The values for these data for the oxidation of the two NiCoCrAlY alloys at 1,373 K are given in Table 1.

In order to verify the model calculations, for both alloys, the minimum, average and maximum oxide-scale thickness, the amount of yttria within a protrusion and the depth of the Ni_5Y-precipitate-free zone were also determined from experiment. For the determination of the Ni_5Y-precipitate-free zone, the amount of Y_2O_3 within a protrusion and the minimum- and maximum-scale thickness, as can be seen in Fig. 4, were determined from backscatter-electron images for at least 25 positions along the O/M interface. For the determination of the average oxide-layer thickness, five BSE images were converted into grayscale images for each alloy. Then the

Table 1 Data used for the calculations. The data apply to the oxidation of a Ni–20Co–19Cr–24Al–0.2Y (at.%) alloy at 1,373 K

Symbol	Value	Unit	Remarks
Molar volume alloy	7.0	cm^3/mol	Taken from Ref. [30]
Molar volume Y_2O_3	44.9	cm^3/mol	Taken from Ref. [31]
Molar volume Al_2O_3	25.6	cm^3/mol	Taken from Ref. [31]
Y content in alloy	0.2	at.%	Measured with EPMA
Y solubility in alloy	0.01	at.%	Half of the EPMA detection limit
Y boundary diffusion coefficient	5×10^{-8}	cm^2/s	Fit parameter
Parabolic rate constant α-Al_2O_3	4.2×10^{-13}	g/cm^4s	Taken from Ref. [32]
Specimen thickness	0.4 (EB-PVD) 2.0 (cast)	mm	Measured after surface preparation
Size of β precipitates in alloy	1.5 (EB-PVD) 40 (cast)	μm	Measured from BSE images (Fig. 3)
Size of Ni_5Y precipitates	1 (EB-PVD) 3 (cast)	μm	Measured from BSE images (Fig. 3)

average oxide-layer thickness was taken equal to the number of pixels belonging to the oxide scale divided by the total number of pixels in the image and multiplied by the height of the image.

Results and Discussion

The experimental and calculated evolution of the minimum, maximum and average oxide-layer thickness for both alloys as function of oxidation time is shown in Fig. 5. Good agreement exists between the experiments and the model calculations.

On the surfaces of both alloys, a continuous, columnar-grain α-Al_2O_3 layer formed between the protrusions (Fig. 2). The generally accepted mechanism for the growth of such an alumina layer is the inward diffusion of oxygen along oxide grain boundaries [33, 34]. If diffusion through the scale is rate-limiting, the experimental growth kinetics can usually be described with a parabolic growth law [9, 10]. Thus, provided that the oxide scales developed between the protrusions do not have different microstructures, for both alloys the growth kinetics should be parabolic and the parabolic rate constant describing the evolution of the minimum oxide-layer thickness should be similar. Indeed, the experimental results for the minimum oxide-layer thickness are well described with the same parabolic rate constant if the transient oxidation period is taken into account (Fig. 5).

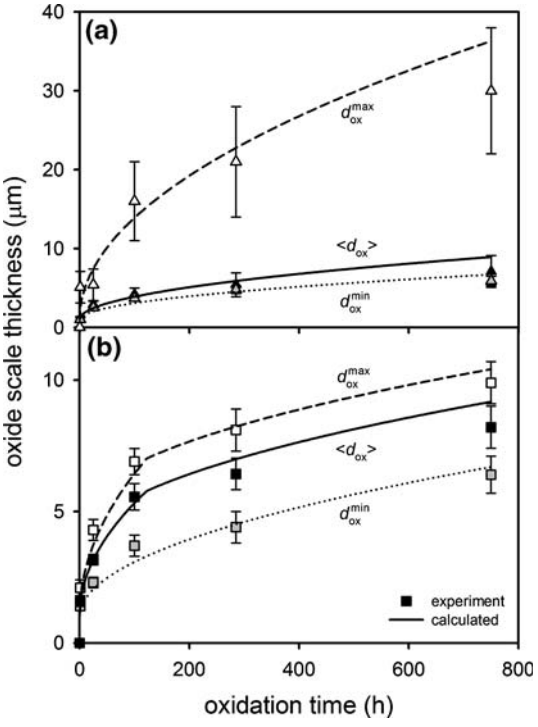

Fig. 5 Experimentally determined and calculated minimum, maximum and average oxide-layer thickness as function of oxidation time for the oxidation of the (**a**) cast, and (**b**) EB-PVD NiCoCrAlY coating at 1,373 K. The data points up to 100 h of oxidation were determined from isothermal-oxidation experiments, the data points at 285 h and 750 h of oxidation were determined from thermal-cycling tests

In the size evolution of the protrusions, considerable differences were observed for the two alloys. Clearly, the maximum oxide-layer thickness is much smaller for the EB-PVD coating (Fig. 5b). This is attributed to the fact that the EB-PVD coating contains a high density of grain and phase boundaries at which small Ni_5Y precipitates are present (Figs. 1b and 3b). Subsequent oxidation leads to the formation of a high density of Y-oxide inclusions in the scale, but only with a small penetration of the oxide scale into the alloy (Figs. 2c and d). For the cast alloy, on the other hand, the Ni_5Y precipitates are much larger, and therefore the penetration of the oxide scale into the alloy is much deeper (Figs. 2b and 5a). However, due to the large size of the β precipitates, the distance between two protrusions in the cast alloy is much larger than that of the EB-PVD coating (Fig. 2b).

Like the minimum oxide-layer thickness, the maximum oxide-layer thickness also shows a parabolic evolution with oxidation time (Fig. 5). The reason for this is that the supply of Y from the alloy towards the oxide scale (i.e. the dissolution of Y from the Ni_5Y precipitates) is controlled by diffusion and thus proportional to the square root of oxidation time (Fig. 6a). For the EB-PVD coating, a transition in the growth kinetics of the protrusions can be observed (Fig. 5b). Clearly, after about 100 h of oxidation, the size of the protrusion increases much slower than before this point. This transition from fast to slow kinetics is attributed to the total depletion of Ni_5Y precipitates from the EB-PVD coating (Fig. 6a). The complete disappearance of the Ni_5Y precipitates from the coating is associated with a maximum in the size of the Y oxide inclusions in the scale (Fig. 6b). For the cast alloy, no total depletion

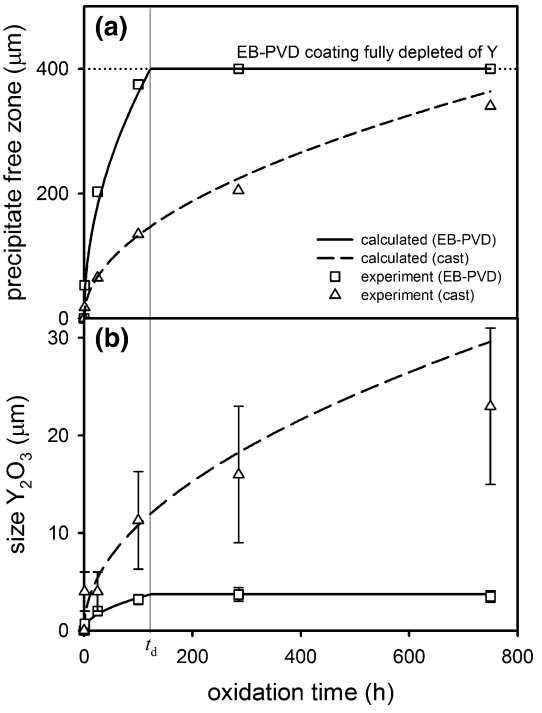

Fig. 6 Experimentally determined and calculated (**a**) depth of the Ni_5Y precipitate-free zone as function of oxidation time, and (**b**) amount of Y_2O_3 within a single peg as a function of oxidation time, for the oxidation of the cast and EB-PVD NiCoCrAlY alloys at 1,373 K. The data points up to 100 h of oxidation were determined from isothermal-oxidation experiments, the data points at 285 h and 750 h of oxidation were determined from a thermal-cycling test

of Y occurred and thus no transition in the growth kinetics of the protrusions was observed. This is attributed to the use of a thicker specimen for the cast alloy (2 mm as compared to 1 mm for the EB-PVD coating) and a slower rate at which the Ni_5Y-precipitate-free zone thickens (Fig. 6a). The latter is an effect of the larger size of the Ni_5Y precipitates in the cast alloy (Fig. 1).

The average oxide-layer growth kinetics are a combination of the oxidation kinetics between and on top of the alloy grain/phase boundaries (see section "Modeling and Data Analysis"). Thus, the average oxide-scale growth rate is determined by the values for the minimum and maximum oxide-layer thickness, as well as the distance between two alloy grain/phase boundaries. Experimental and calculated average oxide-layer growth kinetics in terms of specimen mass gain for the cast alloy and the EB-PVD coating are shown in Fig. 7. Clearly, on average the EB-PVD coating oxidizes faster than the cast alloy when oxidized under the same conditions (i.e. temperature and oxygen partial pressure). This difference in scale growth rate is solely determined by the difference in Y distribution in the two alloys, since both alloys form a continuous α-Al_2O_3 layer with similar amounts of transient oxidation op top of the alloy phases (Fig. 2). Thus, on a NiCoCrAlY alloy, an oxide scale containing a high density of small Y oxide inclusions grows faster than an oxide scale containing only a few, large Y oxide inclusions.

For the oxidation of MCrAlY alloys, our present results have the following implications. First, the average growth kinetics of the scale developing on a MCrAlY alloy will always be faster than that of a pure alumina scale, as long as Y-rich-oxide inclusions become incorporated in the scale. Only after the Y in the coating has been completely consumed, the oxidation rate of a MCrAlY alloy can be described solely by the parabolic rate constant of α-Al_2O_3. Next, the oxidation kinetics of a MCrAlY coating depend on the microstructure of the coating, i.e. Y distribution, and the specimen thickness, i.e. Y reservoir. This is in agreement with previous observations [16, 17]. Finally, if the Y in the coating becomes totally depleted (a phenomenon which will always occur when thin coatings are applied), a transition in the oxidation kinetics will occur. This may explain why the experimental growth kinetics of a MCrAlY coating [12] cannot be described with a single parabolic rate constant.

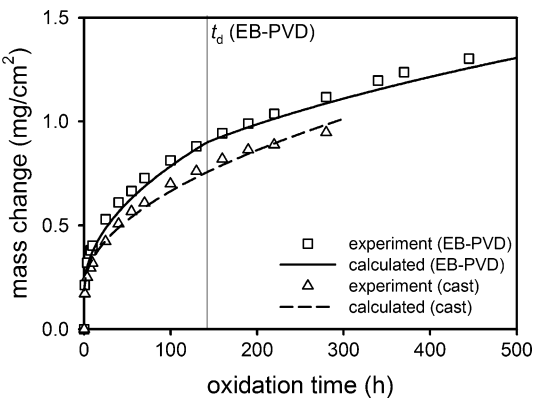

Fig. 7 Experimentally determined and calculated weight change as function of oxidation time for the oxidation of cast and the EB-PVD NiCoCrAlY alloy at 1,373 K. The calculated data represent the isothermal oxidation kinetics, the experimental data are results from a thermal-cycle test up to the point where oxide spallation was first observed

Conclusions

The relation between the Y distribution in the alloy and the growth kinetics of the developing oxide scale was studied for the thermal oxidation of two Ni–20Co–19Cr–24Al–0.2Y (at.%) alloys at 1,373 K: (i) a coarse grain cast alloy with large Ni_5Y intermetallic precipitates, and (ii) a fine-grain freestanding coating with small Ni_5Y precipitates. Upon isothermal and cyclic oxidation, on both alloys a double-layered oxide developed, consisting of a transient outer layer and an α-Al_2O_3 inner layer containing Y_2O_3 and $YAlO_3$ inclusions (pegs). On top of the coarse-grain cast alloy, only a few, very large pegs formed, whereas on top of the fine-grain freestanding coating a high density of small pegs developed.

It was shown that the average growth kinetics of an oxide scale with Y-rich oxide inclusions is faster than the growth kinetics of an oxide scale consisting of pure α-Al_2O_3. The evolution of the growth kinetics depends on the size and distribution of Y oxide inclusions in the α-Al_2O_3 layer. The NiCoCrAlY alloy oxidizes faster if the developing alumina scale contains a high density of small Y oxide inclusions. For a thin coating, the Y oxide inclusions in the scale attain their maximum size after the Y in the coating is completely consumed. After this point, a decrease in the average oxidation kinetics occurs. This implies that the oxidation rate of a MCrAlY alloy is affected by the specimen thickness.

Acknowledgments This research was carried out under project number MC7.04186 in the framework of the Strategic Research program of the Netherlands Institute for Metals Research in the Netherlands (www.nimr.nl). The authors are indebted to Dr. Ir. A.B. Kloosterman at NLR for thermal cycling testing.

References

1. N. P. Padture, M. Gell, and E. H. Jordan, *Science* **296**, 280 (2002).
2. J. R. Nicholls, *MRS Bulletin* **28**, 659 (2003).
3. M. Peters, C. Leyens, U. Schulz, and W. A. Kaysser, *Advanced Engineering Materials* **3**, 193 (2001).
4. M. J. Stiger, N. M. Yanar, M. G. Topping, F. S. Pettit, and G. H. Meier, *Zeitschrift für Metallkunde* **90**, 1069 (1999).
5. A. G. Evans, D. R. Mumm, J. W. Hutchinson, G. H. Meier, and F. S. Pettit, *Progress in Materials Science* **46**, 505 (2001).
6. V. K. Tolpygo, D. R. Clarke, and K. S. Murphy, *Surface and Coatings Technology* **146–147**, 124 (2001).
7. T. J. Nijdam, G. H. Marijnissen, E. Vergeldt, A. B. Kloosterman and W. G. Sloof, *Oxidation of Metals* **66**, 269 (2006).
8. I. T. Spitsberg, D. R. Mumm, and A. G. Evans, *Materials Science and Engineering A* **394**, 176 (2005).
9. P. Kofstad, *High Temperature Corrosion* (Elsevier Applied Science, London and New York, 1988), p. 162.
10. N. Birks, G. H. Meier, and F. S. Pettit, *Introduction to the High Temperature Oxidation of Metals*, 2nd ed. (Cambridge university press, Cambridge, 2006), p. 39.

11. S. Sridharan, L. Xie, E. H. Jordan, M. Gell, and K. S. Murphy, *Materials Science and Engineering A* **393**, 51 (2005).
12. U. Schulz, M. Menzebach, C. Leyens, and Y. Q. Yang, *Surface and Coatings Technology* **146–147**, 117 (2001).
13. D. R. Mumm and A. G. Evans, *Acta Materialia* **48**, 1815 (2000).
14. J. A. Haynes, M. K. Ferber, W. D. Porter, and E. D. Rigney, *Oxidation of Metals* **52**, 31 (1999).
15. D. P. Whittle, D. H. Boone, and I. M. Allam, *Thin Solid Films* **73**, 359 (1980).
16. J. Toscano, R. Vassen, A. Gil, M. Subanovic, D. Naumenko, L. Singheiser, and W. J. Quadakkers, *Surface and Coatings Technology* **201**, 3906 (2006).
17. T. J. Nijdam, C. Kwakernaak, and W. G. Sloof, *Metallurgical and Materials Transactions* **37A**, 683 (2006).
18. T. J. Nijdam, L. P. H. Jeurgens, J. H. Chen, and W. G. Sloof, *Oxidation of Metals* **64**, 357 (2005).
19. H. Hindam and D. P. Whittle, *Journal of the Electrochemical Society* **129**, 1147 (1982).
20. T. J. Nijdam and W. G. Sloof, *Acta Materialia* **55**, 5980 (2007).
21. C. Kwakernaak, T. J. Nijdam, and W. G. Sloof, *Metallurgical and Materials Transactions* **37A**, 695 (2006).
22. T. J. Nijdam, L. P. H. Jeurgens, and W. G. Sloof, *Acta Materialia* **53**, 1643 (2005).
23. M. Shibata, *JEOL news* **39**, 28 (2004).
24. R. Autrata, P. Schauer, J. Kvapil, and J. Kvapil, *Journal of Physics E: Scientific Instruments* **11**, 707 (1978).
25. C. G. Levi, E. Sommer, S. G. Terry, A. Catanoiu, and M. Rühle, *Journal of the American Ceramic Society* **86**, 676 (2003).
26. D. Clemens, V. Vosberg, L. W. Hobbs, U. Breuer, W. J. Quadakkers, and H. Nickel, *Fresenius Journal of Analytical Chemistry* **355**, 703 (1996).
27. D. Clemens, V. R. Vosberg, H. J. Penkalla, U. Breuer, W. J. Quadakkers, and H. Nickel, *Fresenius Journal of Analytical Chemistry* **358**, 122 (1997).
28. R. Munoz-Arroyo, D. Clemens, F. Tietz, R. Anton, J. Quadakkers, and L. Singheiser, *Materials Science Forum* **369–372**, 165 (2001).
29. C. Mennicke, M.-Y. He, D. R. Clarke, and J. S. Smith, *Acta Materialia* **48**, 2941 (2000).
30. K. A. Khor and Y. W. Gu, *Materials Science and Engineering A* **277**, 64 (2000).
31. O. Kubaschewski and B. E. Hopkins, *Oxidation of Metals and Alloys*, 2nd ed. (Butterworths, London, 1962), p. 8.
32. M. W. Brumm and H. J. Grabke, *Corrosion Science* **33**, 1677 (1992).
33. R. Prescott and M. J. Graham, *Oxidation of Metals* **38**, 233 (1992).
34. F. H. Stott, G. C. Wood, and J. Stringer, *Oxidation of Metals* **44**, 113 (1995).